

On the Distribution of SINR for Cell-Free Massive MIMO Systems

Baolin Chong, Fengqian Guo, Hancheng Lu, *Senior Member, IEEE* and Langtian Qin

Abstract—Cell-free (CF) massive multiple-input multiple-output (mMIMO) has been considered as a potential technology for Beyond 5G communication systems. However, the performance of CF mMIMO systems has not been well studied. Most existing analytical work on CF mMIMO systems is based on the expected signal-to-interference-plus-noise ratio (SINR). The statistical characteristics of the SINR, which is critical for emerging applications that focus on extreme events, have not been investigated. To address this issue, in this paper, we attempt to obtain the distribution of SINR in CF mMIMO systems. Considering a downlink CF mMIMO system with pilot contamination, we first give the closed-form expression of the SINR. Based on our analytical work on the two components of the SINR, i.e., desired signal and interference-plus-noise, we then derive the probability density function and cumulative distribution function of the SINR under maximum ratio transmission (MRT) and full-pilot zero-forcing (FZF) precoding, respectively. Subsequently, the closed-form expressions for two more sophisticated performance metrics, i.e., achievable rate and outage probability, can be obtained. Finally, we perform Monte Carlo simulations to validate our analytical work. The results demonstrate the effectiveness of the derived SINR distribution, achievable rate, and outage probability.

Index Terms—Cell-free (CF) massive multiple-input multiple-output (mMIMO), Signal-to-interference-plus-noise ratio (SINR), maximum ratio transmission (MRT), full-pilot zero-forcing (FZF)

I. INTRODUCTION

Multiple-input multiple-output (MIMO) technology has been extensively deployed in current communication systems to support diverse service types [1]–[3]. However, the arrival of Beyond 5G has introduced a multitude of emerging applications, such as holographic telepresence, augmented reality, virtual reality, and the Internet of everything [4], which have imposed more stringent demands on system performance. The traditional cell-centric MIMO-based cellular networks have become inadequate to meet the demands of the current advancements. In traditional cellular networks, where users within a cell are served by a single base station (BS), users at the cell edge often experience considerable inter-cell interference caused by signals from neighboring cells. Hence, inter-cell interference is an important factor limiting the capacity of cellular networks [5]. Furthermore, users located at different positions within the cellular network

face challenges in receiving uniform service due to varying distances from the BS.

To overcome aforementioned issues, cell-free (CF) massive MIMO (mMIMO) has been proposed, which combines the advantages of mMIMO and distributed MIMO [6]. In a CF mMIMO system, a central processing unit (CPU) is employed to control multiple access points (APs), enabling the concurrent service of multiple users on the same time-frequency resources [4], [7]. Particularly, the distributed deployment of multiple APs eliminates the cell boundaries and reduces the distance between APs and users [8], with which inconsistent service quality and large-scale fading effects can be effectively avoided. It has been proved both spectral efficiency (SE) [9] and energy efficiency (EE) [10] are substantially improved in the CF mMIMO systems.

The significant technical advantages demonstrated by CF mMIMO have spurred an increased research focus on its performance analysis. For CF mMIMO systems under maximum ratio transmission (MRT) precoding, the derivation of expected signal-to-interference-plus-noise ratio (SINR) was initially undertaken by authors of [11]. Subsequently, in [12] and [13], the CF mMIMO system's performance is investigated under downlink and uplink data transmission scenarios with different zero-forcing (ZF) precoding and combining schemes. The performance has also been studied for CF mMIMO systems with other linear receivers, e.g., minimum mean square error (MMSE) receiver [14]. In [15], the analytical work was extended to encompass multi-antenna users, coherent Rayleigh fading channels, and achievable rate, building upon previous considerations of single-antenna users and Rayleigh fading channels. The impact of asynchronous reception of signals by users, resulting from the distributed deployment of APs, was addressed in [16], where a closed-form expression for SE was derived. Another aspect of performance analysis focused on the practicality of CF mMIMO systems. In [17], a stochastic geometry approach was utilized to model the locations of APs in CF mMIMO systems, and an expression for achievable rates was derived. Furthermore, authors in [18] and [19] investigated the impact of mobility and oscillator phase noise on system performance, respectively. In [20], authors considered limited feedback capacity as well as hardware impairments in both APs and users, which leads to the derivation of the corresponding expected SINR. Moreover, the performance of CF mMIMO with other technologies, including low-resolution analog-to-digital converter (ADC) [21], reconfigurable intelligent surfaces (RIS) [22], simultaneous wireless information and power transfer (SWIPT) [23], non-orthogonal multiple access (NOMA) [24], and rate-splitting multiple-access (RSMA)

Baolin Chong, Fengqian Guo, Hancheng Lu and Langtian Qin are with the Department of Electronic Engineering and Information Science, University of Science and Technology of China, Hefei 230027, China. (e-mail: chongbaolin@mail.ustc.edu.cn; fqguo@ustc.edu.cn; hclu@ustc.edu.cn; qlt315@mail@mail.ustc.edu.cn)

[25], has also been extensively studied.

Existing analytical work provides a comprehensive and detailed characterization of the average performance of CF mMIMO systems. However, capturing the statistical properties of the SINR, which is a critical task in CF mMIMO systems applied for emerging applications that focus on extreme events, has not been addressed. The exploration of SINR distribution has been a prominent research topic in MIMO systems. The SINR distribution for MMSE MIMO systems was derived by authors of [26], and subsequent advancements by [27] resulted in the derivation of the exact SINR distribution. Based on the analyzed SINR distribution, numerous research has delved into the performance evaluation of MIMO systems, encompassing metrics such as SE and EE [28], uncoded error and outage probabilities, diversity-multiplexing gain tradeoff, and coding gain [29]. As MIMO systems evolve into CF mMIMO systems, the foundational performance analysis concerning SINR distribution continues to be deficient. Besides, based on the existing research on the expected SINR, only the lower performance bounds of the CF mMIMO system can be obtained, such as the lower bound of achievable rates. However, this fails to exactly reflect the actual system performance. To more precisely characterize the system's performance, it becomes imperative to acquire the SINR distribution. Furthermore, for emerging applications focused on ultra-reliable low-latency communication, such as intelligent driving, remote healthcare, and tactile internet, analyzing the system's performance under extreme conditions becomes even more crucial, clearly going beyond what can be achieved by relying solely on the expected SINR. Analyzing the statistical performance of the CF mMIMO system becomes paramount in such cases. Analyzing the distribution of SINR is becoming increasingly crucial. While there are already existing studies on the distribution of signal-to-noise ratio (SNR) in CF mMIMO systems [30], [31], the impact of interference remains challenging to disregard in many cases. Therefore, conducting research on the statistical properties of SINR in CF mMIMO systems is necessary to gain a deeper understanding of their characteristics.

In this paper, we investigate the statistical characteristics of the SINR in CF mMIMO systems. It should be noted that such analytical work is non-trivial. The dense deployment of APs introduces complexities due to the increased number of signals received by all users. These signals include both target signals and interference signals originating from multiple APs. Each received signal represents the accumulation of numerous individual signals, resulting in intricate interactions among different signals. Furthermore, the reuse of pilot sequences among different users in the system leads to channel estimation correlation between them. The correlation introduces coherence in the precoding vectors and causes the signals transmitted to users employing the same pilot to exhibit coherence. We overcome the aforementioned challenges and obtain the distribution of the SINR in CF mMIMO systems. The main contributions are summarized as follows:

- We consider data transmission in a downlink CF mMIMO system with pilot contamination. Based on the received signals at the users, we give the expressions of the SINR

when MRT and full-pilot ZF (FZF) precoding schemes are involved.

- We conduct an analysis of the SINR distribution under MRT and FZF precoding. Specifically, we begin by decomposing the SINR into two components: the desired signal (DS) and the interference plus noise (IN). For MRT precoding, we leverage the Central Limit Theorem (CLT) and random matrix theory to separately analyze the distributions of DS and IN. This allows us to derive the PDF and CDF of SINR, taking into account the independence between DS and IN. In the case of FZF precoding, we directly compute the distribution of DS and analyze the distribution of IN accordingly. Subsequently, we derive the overall distribution of SINR based on these individual components.
- In order to compare with the lower bound of the achievable rate, we derive closed-form expressions for the achievable rate and the outage probability based on our analytical work on the SINR distribution under the MRT and FZF precoding, respectively. To validate our derived results, we conduct Monte Carlo simulations. The simulation results demonstrate the effectiveness of our analytical work on the distribution of SINR, achievable rate, and outage probability.

The rest of the paper is organized as follows. Section II gives the downlink CF mMIMO system with pilot contamination and the expression of SINR. The distribution of SINR under MRT and FZF precoding for the CF mMIMO system is obtained in Section III, respectively. Section IV gives closed-form expressions for the achievable rate and the outage probability under the MRT and FZF precoding, respectively. Section V presents the simulation results and analysis. Finally, the conclusion is drawn in Section VI.

Notations: In this paper, vectors, and matrices are denoted by lowercase and uppercase bold letters, respectively. For a general matrix \mathbf{A} , \mathbf{A}^H and \mathbf{A}^{-1} represent the Hermitian and inverse of \mathbf{A} , respectively. $|\cdot|$ and $(\cdot)^*$ denote the modulus and the conjugate of a complex number, respectively. $\|\mathbf{x}\|$ denotes ℓ_2 norm of vector \mathbf{x} and $\mathbb{C}^{x \times y}$ represents the space of $x \times y$ complex number matrices. $\mathbb{E}\{x\}$ denote the expected value of x and the calligraphy upper-case letter, such as \mathcal{K} , denotes a set.

II. SYSTEM MODEL

We consider a downlink CF mMIMO system operating in time-division duplex (TDD), where a total of M APs, each equipped with N antennas, have the capability to jointly and coherently serve K users, each equipped with a single antenna. The set of APs and users are denoted by \mathcal{M} and \mathcal{K} , respectively. All APs are connected to a CPU through backhalls. The channel vector \mathbf{h}_{mk} between AP m and user k is modeled as

$$\mathbf{h}_{mk} = \beta_{mk}^{\frac{1}{2}} \mathbf{g}_{mk}, \quad (1)$$

where β_{mk} represents the large-scale fading coefficient which is influenced by path loss and shadowing fading, and $\mathbf{g}_{mk} \sim \mathcal{CN}(0, \mathbf{I}_N)$ denotes the small-scale fading. Table I lists a compilation of the main notations used in this paper.

TABLE I
LIST OF KEY NOTATIONS

Symbol	Description
\mathcal{M}, \mathcal{K}	Index set of APs and users
N	Number of antennas each AP
\mathbf{h}_{mk}	Actual channel between AP m and user k
$\hat{\mathbf{h}}_{mk}$	Estimated channel between AP m and user k
$\tilde{\mathbf{h}}_{mk}$	Channel estimated error between AP m and user k
$\bar{\mathbf{H}}_m$	Full-rank matrix of channel estimates at AP m
β_{mk}	Large scale fading between AP m and user k
c_{mk}	Estimated large scale fading between AP m and user k
l_p	Length of pilot sequence
\mathcal{P}_k	Index set of users which use the same pilot sequence with user k
ρ_p, ρ_d	Normalized pilot power and normalized downlink transmission power each AP
\mathbf{b}_{mk}	Precoding matrix at AP m for user k
DS_k, IN_k	DS and IN for user k

A. Uplink Training and Channel Estimation

During the uplink training phase, each user simultaneously transmits a pilot sequence to all APs, with the length of the pilot sequence denoted as l_p . Define $i_k \in \{1, \dots, l_p\}$ as the index of the pilot used by user k , represented by $\phi_{i_k} \in \mathbb{C}^{l_p \times 1}$. We assume that $l_p \leq K$, which indicates that some users will share the same pilot sequence. Consequently, we define $\mathcal{P}_k \subset \mathcal{K}$ as the set of indices, including k , corresponding to users assigned the same pilot as user k . Therefore, for any user k_1 where $k_1 \neq k$, the condition $i_k = i_{k_1} \Leftrightarrow k_1 \in \mathcal{P}_k$ holds true. The pilot sequences are mutually orthogonal and the inner product of pilot sequences is given by

$$\phi_{i_{k_1}}^H \phi_{i_k} = \begin{cases} 0, & k_1 \notin \mathcal{P}_k, \\ l_p, & k_1 \in \mathcal{P}_k. \end{cases} \quad (2)$$

The pilot signal received by AP m , denoted as \mathbf{Y}_m^p , can be expressed as

$$\mathbf{Y}_m^p = \sqrt{\rho_p} \sum_{k \in \mathcal{K}} \mathbf{h}_{mk} \phi_{i_k}^H + \mathbf{Z}_m^p, \quad (3)$$

where ρ_p denotes the normalized pilot power, and $\mathbf{Z}_m^p \in \mathbb{C}^{N \times l_p}$ corresponds to the additive Gaussian noise matrix at AP m during the uplink training phase, each element of which is independent and follows the distribution of $\mathcal{CN}(0, 1)$.

To estimate the channel to user k , AP m performs a correlation operation between the received pilot signal and the corresponding pilot sequence ϕ_{i_k} . Subsequently, it applies the MMSE technique to obtain the MMSE channel estimate $\hat{\mathbf{h}}_{mk}$ [12], which can be calculated as

$$\hat{\mathbf{h}}_{mk} = \kappa_{mk} \mathbf{Y}_m^p \phi_{i_k}, \quad (4)$$

where κ_{mk} is defined as

$$\kappa_{mk} = \frac{\sqrt{\rho_p} \beta_{mk}}{l_p \rho_p \sum_{k_1 \in \mathcal{P}_k} \beta_{mk_1} + 1}. \quad (5)$$

The channel estimation follows the distribution of $\mathcal{CN}(0, c_{mk} \mathbf{I}_N)$ with c_{mk} given by [12]

$$c_{mk} = \frac{l_p \rho_p \beta_{mk}^2}{l_p \rho_p \sum_{k_1 \in \mathcal{P}_k} \beta_{mk_1} + 1}. \quad (6)$$

Then, denote $\tilde{\mathbf{h}}_{mk} = \mathbf{h}_{mk} - \hat{\mathbf{h}}_{mk}$ as the channel estimation error, which is independent of $\hat{\mathbf{h}}_{mk}$ and follows the distribution of $\mathcal{CN}(0, (\beta_{mk} - c_{mk}) \mathbf{I}_N)$. When multiple users share the same pilot sequence, their channel estimates are parallel to each other. This relationship can be expressed as

$$\hat{\mathbf{h}}_{mk} = \frac{\beta_{mk}}{\beta_{mk_1}} \hat{\mathbf{h}}_{mk_1}, \quad k_1 \in \mathcal{P}_k. \quad (7)$$

B. Downlink Data Transmission

During downlink data training, all APs transmit signals to all users. The signal transmitted by AP m is given by

$$\mathbf{y}_m^d = \sqrt{\rho_d} \sum_{k \in \mathcal{K}} \sqrt{\eta_{mk}} \mathbf{b}_{mk} q_k, \quad (8)$$

where ρ_d represents the normalized downlink transmission power each AP and η_{mk} denotes power control coefficient from AP m to user k . The symbol q_k , which satisfies $\mathbb{E}\{|q_k|^2\} = 1$, is the symbol intended for the user k during downlink data transmission and \mathbf{b}_{mk} is precoding vector.

The precoding vector \mathbf{b}_{mk} for user k at AP m is determined based on the channel estimation. The matrix of the channel estimates, $\hat{\mathbf{H}}_m = [\hat{\mathbf{h}}_{m1}, \hat{\mathbf{h}}_{m2}, \dots, \hat{\mathbf{h}}_{mK}] \in \mathbb{C}^{N \times K}$, is rank-deficient due to the pilot sequence length being smaller than the number of users. To obtain a full-rank matrix of channel estimates, denoted as $\bar{\mathbf{H}}_m \in \mathbb{C}^{N \times l_p}$, we define $\bar{\mathbf{H}}_m = \mathbf{Y}_m^p \Phi$, where $\Phi = [\phi_1, \dots, \phi_{l_p}] \in \mathbb{C}^{l_p \times l_p}$ is the pilot-book matrix [12]. The channel estimate between AP m and user k can be expressed in terms of $\bar{\mathbf{H}}_m$ as

$$\hat{\mathbf{h}}_{mk} = \kappa_{mk} \bar{\mathbf{H}}_m \mathbf{e}_{i_k}, \quad (9)$$

where \mathbf{e}_k represent the i_k th column of unit matrix \mathbf{I}_{l_p} . We consider using MRT and FZF precoding during downlink data transmission [11], [12], the precoding vector \mathbf{b}_{mk} for user k can be expressed as follows:

$$\mathbf{b}_{mk} = \begin{cases} \frac{\bar{\mathbf{H}}_m \mathbf{e}_{i_k}}{\sqrt{\mathbb{E}\{\|\bar{\mathbf{H}}_m \mathbf{e}_{i_k}\|^2\}}}, & \text{MRT,} \\ \frac{\bar{\mathbf{H}}_m (\bar{\mathbf{H}}_m^H \bar{\mathbf{H}}_m)^{-1} \mathbf{e}_{i_k}}{\sqrt{\mathbb{E}\{\|\bar{\mathbf{H}}_m [\bar{\mathbf{H}}_m^H \bar{\mathbf{H}}_m]^{-1} \mathbf{e}_{i_k}\|^2\}}}, & \text{FZF.} \end{cases} \quad (10)$$

Each user receives the signals from all APs and the received signal at user k is

$$r_k^d = \sqrt{\rho_d} \sum_{m \in \mathcal{M}} \sum_{k_1 \in \mathcal{K}} \sqrt{\eta_{mk_1}} \mathbf{h}_{mk_1}^H \mathbf{b}_{mk_1} q_{k_1} + z_k, \quad (11)$$

where z_k is the noise at user k with the distribution of $\mathcal{CN}(0, 1)$. Then, the SINR of user k during downlink data transmission is given in (12).

III. DISTRIBUTION OF SINR FOR CF mMIMO SYSTEM

In this section, we derive the distribution of the SINR for the CF mMIMO system. To begin, we partition the received signal from the user into two components: the DS and the IN, utilizing the expression of SINR. Subsequently, we investigate

$$\gamma_k = \frac{\rho_d \left| \sum_{m \in \mathcal{M}} \sqrt{\eta_{mk}} \hat{\mathbf{h}}_{mk}^H \mathbf{b}_{mk} \right|^2}{\rho_d \sum_{k_1 \neq k} \left| \sum_{m \in \mathcal{M}} \sqrt{\eta_{mk_1}} \hat{\mathbf{h}}_{mk_1}^H \mathbf{b}_{mk_1} \right|^2 + \rho_d \sum_{k_1 \in \mathcal{K}} \left| \sum_{m \in \mathcal{M}} \sqrt{\eta_{mk_1}} \bar{\mathbf{h}}_{mk_1}^H \mathbf{b}_{mk_1} \right|^2 + z_k}. \quad (12)$$

the distribution of DS and IN under the MRT precoding scheme, employing the CLT and random matrix theory. By leveraging the independence properties of DS and IN, we obtain the distribution of SINR. Furthermore, we proceed to change the precoding vector, transitioning to the FZF scheme. We calculate the value of DS and obtain the distribution of IN. Finally, based on the aforementioned analysis regarding DS and IN, we derive the distribution of SINR for the CF mMIMO system.

Based on the expression of SINR for user k , we divide the signal that user k received into DS and IN. Then the expression of SINR γ_k can be represented as

$$\gamma_k = \frac{\text{DS}_k}{\text{IN}_k} = \frac{\rho_d U_k^1}{\rho_d \sum_{k_1 \neq k} U_{kk_1}^2 + \rho_d \sum_{k_1 \in \mathcal{K}} U_{kk_1}^3 + z_k}, \quad (13)$$

where DS_k and IN_k represent the DS and IN for user k . The expression of DS_k and IN_k is given as follows:

$$\begin{aligned} \text{DS}_k &= \rho_d U_k^1, \\ \text{IN}_k &= \rho_d \sum_{k_1 \neq k} U_{kk_1}^2 + \rho_d \sum_{k_1 \in \mathcal{K}} U_{kk_1}^3 + z_k, \end{aligned} \quad (14)$$

The expression of U_k^1 , $U_{kk_1}^2$ and $U_{kk_1}^3$ are given by

$$U_k^1 = \left| \sum_{m \in \mathcal{M}} \sqrt{\eta_{mk}} \hat{\mathbf{h}}_{mk}^H \mathbf{b}_{mk} \right|^2, \quad (15a)$$

$$U_{kk_1}^2 = \left| \sum_{m \in \mathcal{M}} \sqrt{\eta_{mk_1}} \hat{\mathbf{h}}_{mk_1}^H \mathbf{b}_{mk_1} \right|^2, \quad (15b)$$

$$U_{kk_1}^3 = \left| \sum_{m \in \mathcal{M}} \sqrt{\eta_{mk_1}} \bar{\mathbf{h}}_{mk_1}^H \mathbf{b}_{mk_1} \right|^2. \quad (15c)$$

For the convenience of the following analysis, we redefine $U_k^1 = |\xi_{mk}|^2$, $U_k^2 = |\xi_{mkk_1}|^2$ and $U_k^3 = |\psi_{mkk_1}|^2$, where ξ_{mk} , ξ_{mkk_1} and ψ_{mkk_1} is given by $\xi_{mk} = \sqrt{\eta_{mk}} \hat{\mathbf{h}}_{mk}^H \mathbf{b}_{mk}$, $\xi_{mkk_1} = \sqrt{\eta_{mk_1}} \hat{\mathbf{h}}_{mk_1}^H \mathbf{b}_{mk_1}$ and $\psi_{mkk_1} = \sqrt{\eta_{mk_1}} \bar{\mathbf{h}}_{mk_1}^H \mathbf{b}_{mk_1}$, respectively.

A. Maximum Ratio Transmission

In this subsection, we derive the distribution of SINR when MRT precoding is used. In the presence of multiple users receiving signals from all APs simultaneously, it becomes evident from equation (12) that all signals are interconnected, giving rise to the formation of the DS and the IN. Consequently, directly analyzing the distribution of SINR under MRT precoding is a challenging task. To overcome this difficulty, we adopt a feasible approach in the subsequent analysis. Firstly, we scrutinize the expressions for the distribution of DS and IN individually. Subsequently, by utilizing the derived expressions for the distributions of DS and IN, we are able to obtain the distribution of SINR.

When the number of APs M and number of antennas at each AP N are large enough, the distribution of $\sum_{m \in \mathcal{M}} \sqrt{\eta_{mk}} \hat{\mathbf{h}}_{mk}^H \mathbf{b}_{mk}$ is approximated as a Gaussian distribution. Then we can approximate U_k^1 as a Gamma distribution in the following lemma.

Lemma 1. *When MRT precoding is used for downlink data transmission, the distribution of U_k^1 can be approximated as a Gamma distribution with the shape parameter j_{k1} and the scale parameter χ_{k1} , i.e., $U_k^1 \sim \text{Gamma}(j_{k1}, \chi_{k1})$. Therefore, the PDF and cumulative distribution function (CDF) of U_k^1 is expressed as follows:*

$$\begin{cases} f_{U_k^1}(x) = \frac{1}{\Gamma(j_{k1}) \chi_{k1}^{j_{k1}}} x^{j_{k1}-1} e^{-\frac{x}{\chi_{k1}}}, \\ F_{U_k^1}(x) = \frac{1}{\Gamma(j_{k1})} \bar{\gamma}\left(j_{k1}, \frac{x}{\chi_{k1}}\right), \end{cases} \quad (16)$$

where $\Gamma(z) = \int_0^{+\infty} t^{z-1} e^{-t} dt$ and $\bar{\gamma}(a, z) = \int_0^z t^{a-1} e^{-t} dt$ represent the gamma function and incomplete gamma function, respectively. The shape parameter j_{k1} and scale parameter χ_{k1} are given by

$$j_{k1} = \frac{u_{U_k^1}^2}{u_{U_k^1}^{(2)} - u_{U_k^1}^2}, \quad \chi_{k1} = \frac{u_{U_k^1}^{(2)} - u_{U_k^1}^2}{u_{U_k^1}}, \quad (17)$$

where $u_{U_k^1} = \mathbb{E}\{U_k^1\}$ and $u_{U_k^1}^{(2)} = \mathbb{E}\{(U_k^1)^2\}$ denote the first and second moments of U_k^1 respectively. The expressions for $u_{U_k^1}$ and $u_{U_k^1}^{(2)}$ are given in (40) and (41), respectively.

Proof. Please refer to Appendix A. \square

Since $\text{DS}_k = \rho_d U_k^1$, we have $\mathbb{E}\{\text{DS}_k\} = \rho_d \mathbb{E}\{U_k^1\}$ and $\mathbb{E}\{\text{DS}_k^2\} = \rho_d \mathbb{E}\{(U_k^1)^2\}$. Then, DS_k^{MRT} can be approximated as a Gamma distribution with shape parameter j_{k1} and scale parameter $\rho_d \chi_{k1}$, i.e., $\text{DS}_k^{\text{MRT}} \sim \text{Gamma}(j_{k1}, \rho_d \chi_{k1})$, where DS_k^{MRT} represents the DS_k with MRT precoding.

Then we turn to analyze the distribution of IN_k^{MRT} , where IN_k^{MRT} represents the IN_k with MRT precoding. Similarly, the distribution of IN_k^{MRT} can be approximated as a Gamma distribution. In the following lemma, we approximate IN_k^{MRT} as a Gamma distribution.

Lemma 2. *When MRT precoding is used for downlink data transmission, the distribution of $\text{IN}_k^{\text{MRT}} = \rho_d \sum_{k_1 \neq k} U_{kk_1}^2 + \rho_d \sum_{k_1 \in \mathcal{K}} U_{kk_1}^3 + z_k$ can be approximated as a Gamma distribution with the shape parameter j_{k2} and the scale parameter χ_{k2} , i.e., $\text{IN}_k^{\text{MRT}} \sim \text{Gamma}(j_{k2}, \chi_{k2})$. The shape parameter j_{k2} and scale parameter χ_{k2} are given by*

$$j_{k2} = \frac{u_{\text{IN}_k^{\text{MRT}}}^2}{u_{\text{IN}_k^{\text{MRT}}}^{(2)} - u_{\text{IN}_k^{\text{MRT}}}^2}, \quad \chi_{k2} = \frac{u_{\text{IN}_k^{\text{MRT}}}^{(2)} - u_{\text{IN}_k^{\text{MRT}}}^2}{u_{\text{IN}_k^{\text{MRT}}}}, \quad (18)$$

where $u_{IN_k^{MRT}} = \mathbb{E} \{ IN_k^{MRT} \}$ and $u_{IN_k^{MRT}}^{(2)} = \mathbb{E} \{ (IN_k^{MRT})^2 \}$ are first and second moments of IN_k^{MRT} , respectively. The expressions for $u_{IN_k^{MRT}}$ and $u_{IN_k^{MRT}}^{(2)}$ are given in (50) and (51), respectively.

Proof. Please refer to Appendix B. \square

Based on the above analysis, we have obtained the distributions of the two components of the SINR: DS and IN. By leveraging the independence property between these two components, we can obtain the distribution of SINR in the CF mMIMO system which is shown in the following theorem.

Theorem 1. *In the CF mMIMO system with pilot contamination, when MRT precoding is used for downlink data transmission, the PDF and CDF of the SINR for user k , $\forall k \in \mathcal{K}$ can be expressed as follows:*

$$\begin{cases} f_{\gamma_k}^{MRT}(x) = \frac{\Gamma(j_{k1} + j_{k2}) x^{j_{k1}-1} \left(\frac{1}{\chi_{k2}} + \frac{x}{\rho_d \chi_{k1}} \right)^{-j_{k1}-j_{k2}}}{\Gamma(j_{k1}) \Gamma(j_{k2}) (\rho_d \chi_{k1})^{j_{k1}} \chi_{k2}^{j_{k2}}}, \\ F_{\gamma_k}^{MRT}(x) = \frac{\Gamma(j_{k1} + j_{k2}) \chi_{k2}^{j_{k1}} x^{j_{k1}}}{j_{k1} \Gamma(j_{k1}) \Gamma(j_{k2}) (\rho_d \chi_{k1})^{j_{k1}}} \\ \quad \times H(j_{k1}, j_{k1} + j_{k2}, j_{k1} + 1, -\frac{\chi_{k2} x}{\rho_d \chi_{k1}}), \end{cases} \quad (19)$$

where j_{k1} , χ_{k1} , j_{k2} , and χ_{k2} are given in Lemma 1 and Lemma 2, respectively, $H(a, b, c)$ is the hypergeometric function [32].

Proof. Please refer to Appendix C. \square

B. Full-Pilot Zero-Forcing

Different from MRT precoding, FZF precoding can suppress inter-user interference. The FZF precoding vector used by AP m towards user k is given in (10), and the denominator of the precoding vector is given in closed form by [12]

$$\begin{aligned} \mathbb{E} \left\{ \left\| \bar{\mathbf{H}}_m [\bar{\mathbf{H}}_m^H \bar{\mathbf{H}}_m]^{-1} \mathbf{e}_{i_k} \right\|^2 \right\} &= \mathbb{E} \left\{ \left[(\bar{\mathbf{H}}_m^H \bar{\mathbf{H}}_m)^{-1} \right]_{i_k i_k} \right\} \\ &\stackrel{(a)}{=} \frac{\kappa_{mk}^2}{(N - l_p) c_{mk}}, \end{aligned} \quad (20)$$

where (a) is obtained based on [33, Lemma 2.10], for a $l_p \times l_p$ central complex Wishart matrix with M degrees of freedom satisfying $M \geq l_p + 1$. Interference between users using different pilot sequences is suppressed and the product between $\hat{\mathbf{h}}_{mk}^H$ and $\mathbf{b}_{mk'}$ can be calculated as follows [12]:

$$\begin{aligned} \alpha_{mkk_1} &= \hat{\mathbf{h}}_{mk}^H \mathbf{b}_{mk_1} \\ &= (\kappa_{mk} \bar{\mathbf{H}}_m \mathbf{e}_{i_k})^H \bar{\mathbf{H}}_m (\bar{\mathbf{H}}_m^H \bar{\mathbf{H}}_m)^{-1} \mathbf{e}_{i_{k_1}} \sqrt{\frac{(N - l_p) c_{mk}}{\kappa_{mk}^2}} \\ &= \begin{cases} 0, & k_1 \notin \mathcal{P}_k, \\ \sqrt{(N - l_p) c_{mk}}, & k_1 \in \mathcal{P}_k. \end{cases} \end{aligned} \quad (21)$$

Then we can obtain the value of DS_k based on (21) as follows:

$$\begin{aligned} DS_k^{FZF} &= \rho_d \left(\sum_{m \in \mathcal{M}} \sqrt{\eta_{mk}} \alpha_{mkk} \right)^2 \\ &= \rho_d \left(\sum_{m \in \mathcal{M}} \sqrt{\eta_{mk} (N - l_p) c_{mk}} \right)^2, \end{aligned} \quad (22)$$

where DS_k^{FZF} represents the DS_k with FZF precoding.

Similar to the analysis under MRT precoding, we approximate the distribution of IN_k^{FZF} under FZF precoding as a Gamma distribution in the following lemma.

Lemma 3. *When FZF precoding is used for downlink data transmission, the distribution of $IN_k^{FZF} = \rho_d \sum_{k_1 \neq k} U_{kk_1}^2 + \rho_d \sum_{k_1 \in \mathcal{K}} U_{kk_1}^3 + z_k$ can be approximated as a Gamma distribution with the shape parameter j_{k2} and the scale parameter χ_{k2} , i.e., $IN_k^{FZF} \sim \text{Gamma}(j_{k2}, \chi_{k2})$. The shape parameter j_{k2} and scale parameter χ_{k2} are given by*

$$j_{k2} = \frac{u_{IN_k^{FZF}}^2}{u_{IN_k^{FZF}}^{(2)} - u_{IN_k^{FZF}}^2}, \quad \chi_{k2} = \frac{u_{IN_k^{FZF}}^{(2)} - u_{IN_k^{FZF}}^2}{u_{IN_k^{FZF}}}, \quad (23)$$

where $u_{IN_k^{FZF}} = \mathbb{E} \{ IN_k^{FZF} \}$ and $u_{IN_k^{FZF}}^{(2)} = \mathbb{E} \{ (IN_k^{FZF})^2 \}$ are first and second moments of IN_k^{FZF} , respectively. The expressions for $u_{IN_k^{FZF}}$ and $u_{IN_k^{FZF}}^{(2)}$ are given in (26) and (27), respectively.

Proof. Define $U_k^2 = \rho_d \sum_{k_1 \neq k} U_{kk_1}^2$, similar to (22), the value of U_k^2 can be expressed as follows:

$$U_k^2 = \rho_d \sum_{k_1 \neq k} \left(\sum_{m \in \mathcal{M}} \sqrt{\eta_{mk_1}} \alpha_{mkk_1} \right)^2. \quad (24)$$

Similar to (48), the second and fourth moment of $\psi_{mkk_1}^d$ can be calculated as follows:

$$\begin{aligned} \mathbb{E} \left\{ |\psi_{mkk_1}|^2 \right\} &= \eta_{mk_1} (\beta_{mk} - c_{mk}) \\ \mathbb{E} \left\{ |\psi_{mkk_1}|^4 \right\} &= \eta_{mk_1}^2 \frac{2(N+1)}{N} (\beta_{mk} - c_{mk})^2 \end{aligned} \quad (25)$$

Then we can obtain the first moment and second moment of $U_{kk_1}^3$ under FZF precoding, i.e., $\mathbb{E} \{ U_{kk_1}^3 \}$, $\mathbb{E} \{ (U_{kk_1}^3)^2 \}$, which is similar to (49) in the proof of Lemma 2. Then first moment of IN_k^{FZF} can be expressed as follows:

$$u_{IN_k^{FZF}} = U_k^2 + \rho_d \sum_{k_1 \in \mathcal{K}} \mathbb{E} \{ U_{kk_1}^3 \} + 1. \quad (26)$$

The second moments of IN_k^{FZF} can be calculated as follows:

$$\begin{aligned} u_{IN_k^{FZF}}^{(2)} &= \rho_d^2 \sum_{k_1 \in \mathcal{K}} \mathbb{E} \left\{ (U_{kk_1}^3)^2 \right\} + 2\rho_d (U_k^2 + 1) \sum_{k_1 \in \mathcal{K}} \mathbb{E} \{ U_{kk_1}^3 \} \\ &\quad + \rho_d^2 \sum_{k_1 \in \mathcal{K}} \sum_{k_2 \neq k_1} \mathbb{E} \{ U_{kk_1}^3 \} \mathbb{E} \{ U_{kk_2}^3 \} + (U_k^2)^2 + 2U_k^2 + 2. \end{aligned} \quad (27)$$

We calculate the value of DS_k^{FZF} and obtain the distribution of IN_k^{FZF} above. Then the distribution of SINR under the FZF precoding can be obtained as shown in the following theorem.

Theorem 2. *In the CF mMIMO system with pilot contamination, when FZF precoding is used for downlink data*

transmission, the PDF and CDF of the SINR for user k , $\forall k \in \mathcal{K}$ can be expressed as follows:

$$\begin{aligned} f_{\gamma_k}^{\text{FZF}}(x) &= \frac{1}{\Gamma(j_{k2})\chi_{k2}^{j_{k2}}x} \left(\frac{DS_k^{\text{FZF}}}{x} \right)^{j_{k2}} e^{-\frac{DS_k^{\text{FZF}}}{x\chi_{k2}}}, \\ F_{\gamma_k}^{\text{FZF}}(x) &= 1 - \frac{1}{\Gamma(j_{k2})} \bar{\gamma} \left(j_{k2}, \frac{DS_k^{\text{FZF}}}{x\chi_{k2}} \right), \end{aligned} \quad (28)$$

where DS_k^{FZF} is given in (22), j_{k2} , and χ_{k2} are given in Lemma 3.

Proof. The CDF of γ_k when using the FZF precoder can be calculated as follows:

$$\begin{aligned} F_{\gamma_k}^{\text{FZF}}(x) &= P \left\{ \frac{DS_k^{\text{FZF}}}{\text{IN}_k^{\text{FZF}}} \leq x \right\} = P \left\{ \text{IN}_k^{\text{FZF}} \geq \frac{DS_k^{\text{FZF}}}{x} \right\} \\ &= 1 - F_{\text{IN}_k^{\text{FZF}}} \left(\frac{DS_k^{\text{FZF}}}{x} \right), \end{aligned} \quad (29)$$

where $F_{\text{IN}_k^{\text{FZF}}}(\cdot)$ represents the CDF of IN_k^{FZF} .

Based on (29), the PDF of γ_k when using FZF precoder can be calculated as follows:

$$\begin{aligned} f_{\gamma_k}^{\text{FZF}}(x) &= \frac{dF_{\gamma_k}^{\text{FZF}}(x)}{dx} = -\frac{dF_{\text{IN}_k^{\text{FZF}}} \left(\frac{DS_k^{\text{FZF}}}{x} \right)}{dx} \\ &= \frac{DS_k^{\text{FZF}}}{x^2} f_{\text{IN}_k^{\text{FZF}}} \left(\frac{DS_k^{\text{FZF}}}{x} \right), \end{aligned} \quad (30)$$

where $f_{\text{IN}_k^{\text{FZF}}}(\cdot)$ represents the PDF of IN_k^{FZF} . \square

IV. PERFORMANCE ANALYSIS

The lower bound of achievable rate for users in the CF mMIMO system has been investigated [12]. However, to provide a more comprehensive characterization of the system's performance, this section focuses on deriving the achievable rate of users under both MRT and FZF precoding. This analysis is based on the previously obtained distribution of SINR, allowing for a more accurate assessment of system performance. Besides, we also derive the outage probability of the CF mMIMO system.

A. Maximum Rate Transmission

When MRT precoding is used in the CF mMIMO system, then the lower bound of achievable downlink rate is given in (33) [12]. The achievable rate in the CF mMIMO system with MRT precoding employed is given in the following lemma.

Lemma 4. *In the CF mMIMO system with pilot contamination, when MRT precoding is employed for downlink data transmission, the achievable rate for user k , $k \in \mathcal{K}$, is given in (35), where $H^P(\{\cdot\}, \{\cdot\}, \{\cdot\})$ represents the generalized hypergeometric function [34]. The values of j_{k1} and χ_{k1} are obtained from Lemma 1, while j_{k2} and χ_{k2} are derived from Lemma 2.*

Proof. When MRT precoding is employed for downlink data transmission, the PDF of SINR for user k , $k \in \mathcal{K}$, is given in Theorem 1. Then the achievable rate for user k can be calculated directly by $R_k^{\text{MRT}} = \int_0^\infty \log_2(1+x) f_{\gamma_k}^{\text{MRT}}(x) dx$. \square

Consider the encoding rate of user k is r_k^{MRT} in the CF mMIMO system under MRT precoding. An outage event for user k when the SINR can't support the target rate r_k^{MRT} . The outage probability of user k in the CF mMIMO system is given by

$$\begin{aligned} P_{\text{out},k}^{\text{MRT}}(r_k^{\text{MRT}}) &= P(\log_2(1 + \gamma_k) \leq r_k^{\text{MRT}}) \\ &= F_{\gamma_k}^{\text{MRT}}(2^{r_k^{\text{MRT}}} - 1). \end{aligned} \quad (31)$$

B. Full-Pilot Zero-Forcing

When FZF precoding is used in the CF mMIMO system, then the lower bound of achievable downlink rate is given (34) [12].

The achievable rate in the CF mMIMO system with FZF precoding employed is given in the following lemma.

Lemma 5. *In the CF mMIMO system with pilot contamination, when FZF precoding is employed for downlink data transmission, the achievable rate for user k , $k \in \mathcal{K}$, is given in (36), where DS_k^{FZF} is given in (22), while j_{k2} and χ_{k2} are obtained from Lemma 3.*

Proof. The proof is similar to the proof of Lemma 4, which is omitted for simplicity. \square

Consider the encoding rate of user k is r_k^{MRT} in the CF mMIMO system under FZF precoding. The outage probability of user k is given by

$$P_{\text{out},k}^{\text{MRT}}(r_k^{\text{MRT}}) = F_{\gamma_k}^{\text{FZF}}(2^{r_k^{\text{MRT}}} - 1). \quad (32)$$

V. SIMULATION RESULTS

In this section, we validate our derived results by conducting Monte Carlo simulations across various scenarios and subsequently perform corresponding performance analysis.

A. Simulation Setting

In our simulations, we consider a system of randomly distributed APs and users within a rectangular area measuring $1\text{km} \times 1\text{km}$. The large-scale fading coefficient, which accounts for both path loss and shadowing effects, is denoted as $\beta_{mn} = PL_{mn} + z_{mn}$, where PL_{mn} represents the path loss component, while $z_{mn} \sim \mathcal{CN}(0, \delta_{sh}^2)$ represents the shadowing component following a complex Gaussian distribution with a mean of zero and a variance of δ_{sh}^2 . To characterize the path loss, we employ a three-slope model proposed in [11] and adopt the same parameter settings as described in that paper. In addition, we set the pilot power to 20 dBm and the downlink transmit power to 23 dBm. The system bandwidth is 2 MHz and the power of Gaussian noise is -174 dB/Hz. The pilots are sequentially assigned to users, i.e., $i_k = \text{rem}(k, l_p)$, where $\text{rem}(\cdot)$ represents the remainder operation. We employ the heuristic power allocation scheme introduced in [12], and the power allocation coefficients are computed using the following equation:

$$\eta_{mk} = \frac{c_{mk}}{\sum_{k \in \mathcal{K}} c_{mk}}, \forall m, \forall k. \quad (37)$$

$$\bar{R}_k^{\text{MRT}} = \log_2 \left(1 + \frac{N \rho_d \left(\sum_{m \in \mathcal{M}} \sqrt{\eta_{mk} c_{mk}} \right)^2}{N \rho_d \sum_{k_1 \in \mathcal{P}_k \setminus \{k\}} \left(\sum_{m \in \mathcal{M}} \sqrt{\eta_{mk} c_{mk}} \right)^2 + \rho_d \sum_{m \in \mathcal{M}} \sum_k^{\mathcal{K}} \eta_{mk} \beta_{mk} + 1} \right). \quad (33)$$

$$\bar{R}_k^{\text{FZF}} = \log_2 \left(1 + \frac{(N - l_p) \rho_d \left(\sum_{m \in \mathcal{M}} \sqrt{\eta_{mk} c_{mk}} \right)^2}{(N - l_p) \rho_d \sum_{k_1 \in \mathcal{P}_k \setminus \{k\}} \left(\sum_{m \in \mathcal{M}} \sqrt{\eta_{mk} c_{mk}} \right)^2 + \rho_d \sum_{m \in \mathcal{M}} \sum_k^{\mathcal{K}} \eta_{mk} \beta_{mk} + 1} \right). \quad (34)$$

$$R_k^{\text{MRT}} = \frac{\pi \csc(j_{k2} \pi)}{\Gamma(j_{k1}) \Gamma(j_{k2}) \ln 2} \left(\frac{(\rho_d \chi_{k1})^{j_{k2}} \Gamma(j_{k1} + j_{k2})}{\chi_{k2}^{j_{k2}} \Gamma(1 + j_{k2})} H(j_{k2}, j_{k1} + j_{k2}, 1 + j_{k2}, \frac{\rho_d \chi_{k1}}{\chi_{k2}}) \right. \\ \left. - \frac{\rho_d \chi_{k1} \Gamma(1 + j_{k1})}{\chi_{k2} \Gamma(2 - j_{k2})} H^P \left(\{1, 1, 1 + j_{k1}\}, \{2, 2 - j_{k2}\}, \frac{\rho_d \chi_{k1}}{\chi_{k2}} \right) \right). \quad (35)$$

$$R_k^{\text{FZF}} = \frac{(-1)^{-j_{k2}} \pi \csc(j_{k2} \pi)}{\Gamma(j_{k2}) \ln 2} \bar{\gamma} \left(-\frac{\text{DS}_k^{\text{FZF}}}{\chi_{k2}}, j_{k2} \right) + \frac{\text{DS}_k^{\text{FZF}} \Gamma(-1 + j_{k2})}{\chi_{k2} \Gamma(j_{k2}) \ln 2} H^P \left(\{1, 1\}, \{2, 2 - j_{k2}\}, \frac{\text{DS}_k^{\text{FZF}}}{\chi_{k2}} \right). \quad (36)$$

For the specific configuration details regarding the number of APs, users, the number of antennas per AP, and the pilot length in the system, we will provide them during the corresponding experiments.

B. CDF of SINR

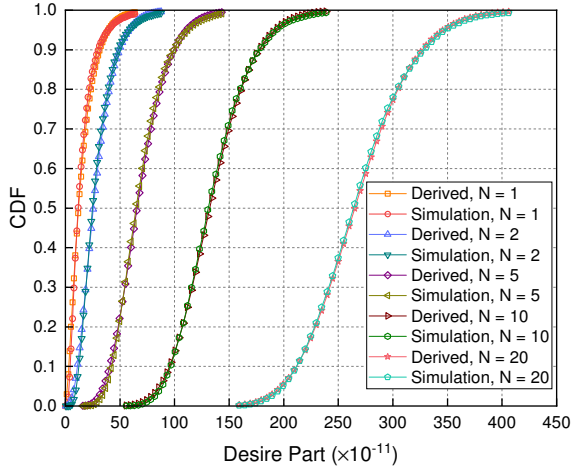


Fig. 1. CDF of DS under MRT precoding with different number of antennas each AP. System parameters: $M = 120$, $K = 20$, $l_p = 10$.

Once MRT precoding is implemented in CF mMIMO systems, the CDF of DS and IN, concerning the variation in the number of antennas at the AP, are illustrated in Fig. 1 and Fig. 2, respectively. As anticipated, both DS and IN exhibit a corresponding increase with the augmentation of antenna quantity. This phenomenon can be attributed to the fact that a higher number of antennas enables the AP to transmit a greater number of signals, consequently leading to an enhancement in signal strength. Furthermore, the results derived from our theoretical analysis align closely with the outcomes obtained through Monte Carlo simulations. This congruence serves as evidence supporting the accuracy of our conclusions.

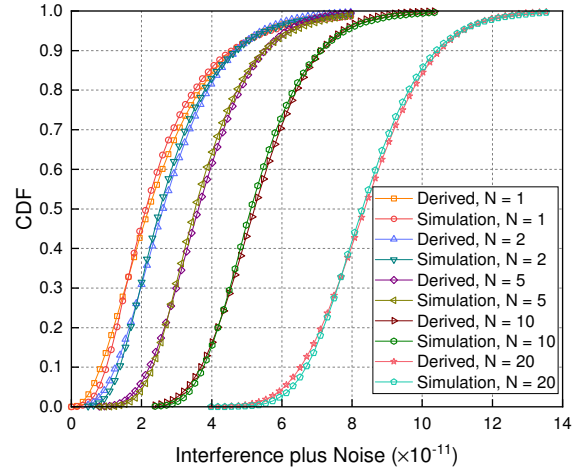


Fig. 2. CDF of IN under MRT precoding with different number of antennas each AP. System parameters: $M = 120$, $K = 20$, $l_p = 10$.

In Fig. 3, we investigate the impact of the variation in the number of antennas at each AP on the CDF of IN when FZF precoding is deployed. As the number of antennas increases at each AP, interference becomes more severe, resulting in a proportional increase of IN. Moreover, the graph illustrates a close alignment between the distribution derived from our theoretical analysis and the distribution obtained through Monte Carlo simulations, providing strong evidence that our conclusions are accurate.

We compare the CDF of the SINR for varying numbers of users under FZF precoding, as illustrated in Fig. 4. It is evident that as the number of users increases, the derived results closely converge with the Monte Carlo simulation results, eventually reaching a consistent agreement. This convergence is attributed to our approximation of the IN based on the CLT. As the number of users grows, this approximation becomes increasingly accurate and approaches the true results. Furthermore, with an increasing number of users, the SINR correspondingly decreases. Despite the unchanged length of the pilot sequence, more users share the same pilot, resulting in significant pilot contamination and subsequently causing

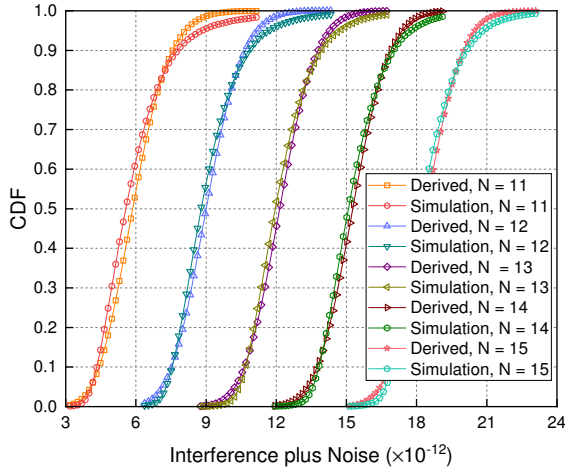


Fig. 3. CDF of IN under FZF precoding with different number of antennas each AP. System parameters: $M = 120$, $K = 20$, $l_p = 10$.

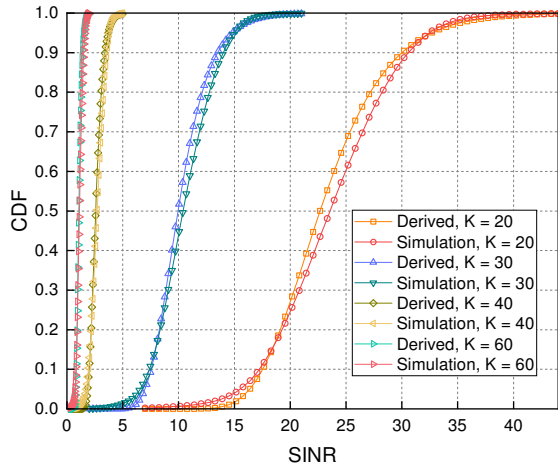


Fig. 4. CDF of SINR under FZF precoding with different number of users. System parameters: $M = 120$, $N = 11$, $l_p = 10$.

severe interference, ultimately leading to a lower SINR.

In Fig. 5, we present the CDF of the SINR under the deployment of MRT precoding, showcasing its variation with respect to the number of users. As the number of users increases, the derived distribution of SINR exhibits a growing consistency with the results obtained from Monte Carlo simulations. This increasing alignment can be attributed to the heightened applicability of the CLT as the number of users expands. Furthermore, similar to the observation in the case of FZF precoding, the SINR decreases with an increasing number of users. The reason for this degradation in SINR is the same. Additionally, under MRT precoding, users who do not employ the same pilot sequence also introduce interference with each other. Consequently, employing FZF precoding in CF mMIMO systems generally yields higher SINR, indicating superior performance compared to MRT precoding.

We turn our attention to comparing the impact of varying the number of antennas on each AP under FZF precoding on the CDF of the SINR in CF mMIMO systems, as depicted in Fig. 6. It is evident that as the number of antennas increases, the derived results align more closely with the results obtained from system analysis. This convergence can be attributed to the increased number of constituent signals in the DS and IN

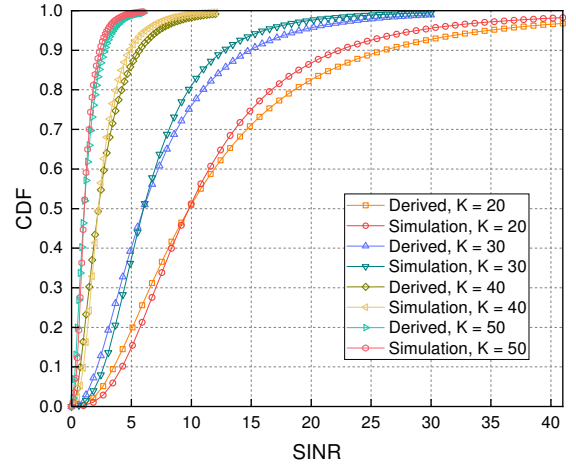


Fig. 5. CDF of SINR under MRT precoding with different number of users. System parameters: $M = 120$, $N = 2$, $l_p = 10$.

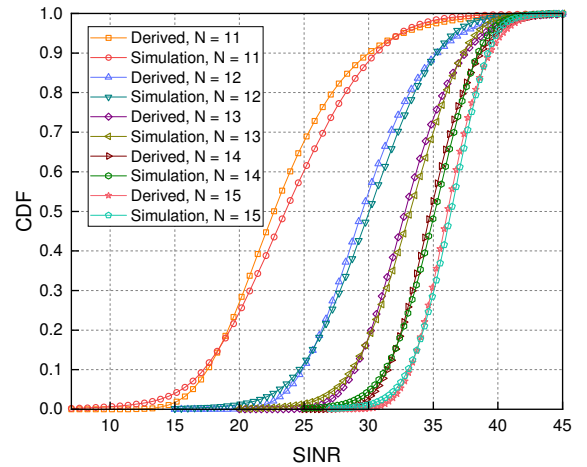


Fig. 6. CDF of SINR under FZF precoding with different number of antennas each AP. System parameters: $M = 120$, $K = 20$, $l_p = 10$.

due to the growing number of antennas, thereby enhancing the accuracy of the approximation based on the CLT. Furthermore, the increase in the number of antennas leads to an increase in SINR. From (22), it can be observed that DS increases with the growing number of antennas. While, according to (24), the $U_{kk_1}^2$ component of IN also increases with the number of users, (25) indicates that $U_{kk_1}^3$ remains unchanged with an increasing number of antennas. Hence, an increase in the number of antennas results in an improvement in SINR.

Fig. 7 illustrates the distribution of SINR under MRT precoding for different numbers of antennas. Similar to the scenario with FZF precoding, it is observed that as the number of antennas increases, the derived CDF of SINR closely aligns with the results obtained from Monte Carlo simulations. Furthermore, an increase in the number of antennas leads to an improvement in SINR. As MRT precoding only mitigates the influence of noise, while FZF precoding suppresses the effects of interference, FZF precoding generally achieves better performance.

C. Achievable Rate and Outage Probability Analysis

We have investigated the impact of varying the number of antennas on each AP and the number of users on achievable

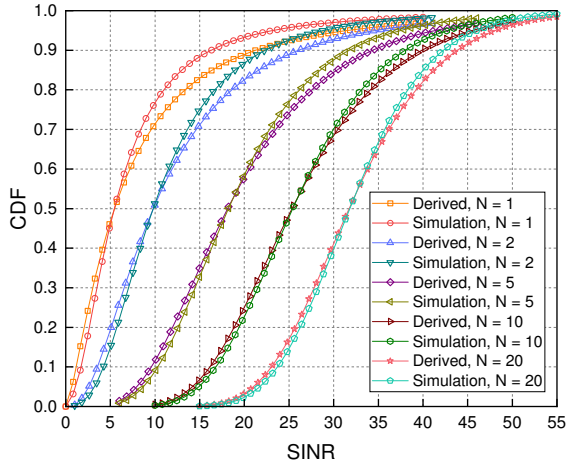


Fig. 7. CDF of SINR under MRT precoding with different number of antennas each AP. System parameters: $M = 120$, $K = 20$, $l_p = 10$.

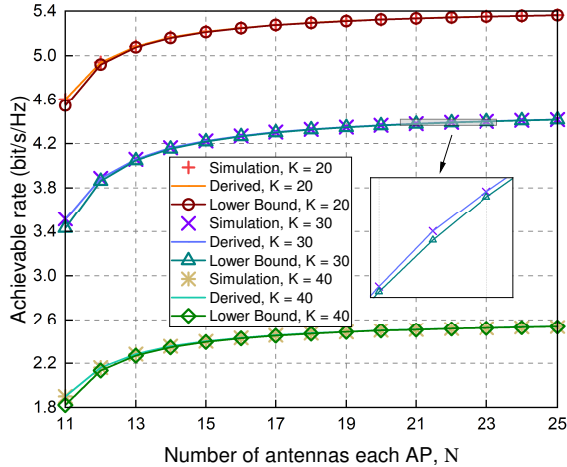


Fig. 8. Achievable rate under FZF precoding with different number of antennas each AP. System parameters: $M = 120$, $l_p = 10$.

rates under both FZF precoding and MRT precoding, as depicted in Fig. 8 and Fig. 9, respectively. It can be observed that the results derived from our analysis align with the results obtained from Monte Carlo simulations. As the number of users decreases and the number of antennas increases, the achievable rates also increase. This is because the reduction in the number of users and the increase in the number of antennas result in higher SINR, thereby leading to an increase in achievable rates. Besides, it can be observed that our derived results are higher than the lower bound with different scenarios. Under MRT precoding, our derived results are significantly higher than the lower bound. However, under FZF precoding, our derived results are only slightly higher than the lower bound. This is because, with FZF precoding, both desired signals and interference can be directly computed, and the uncertainty in SINR mainly comes from channel estimation errors. Therefore, compared to MRT precoding, FZF precoding yields a more stable SINR, resulting in actual achievable rates that are closer to the lower bound.

We conducted separate investigations on the impact of different coding rates and the number of antennas on each AP for outage probability under FZF precoding and MRT precoding, as depicted in Fig. 10 and Fig. 11, respectively.

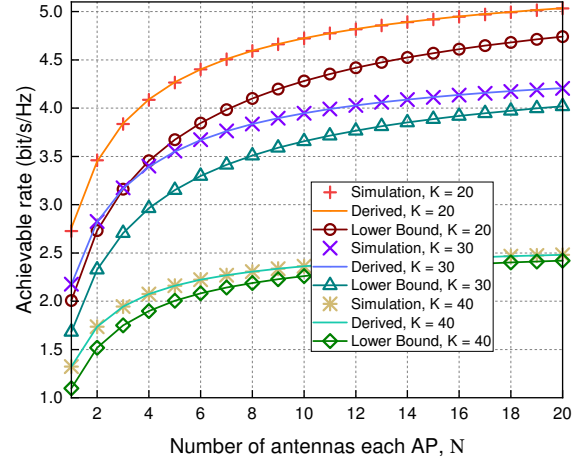


Fig. 9. Achievable rate under MRT precoding with different number of antennas each AP. System parameters: $M = 120$, $l_p = 10$.

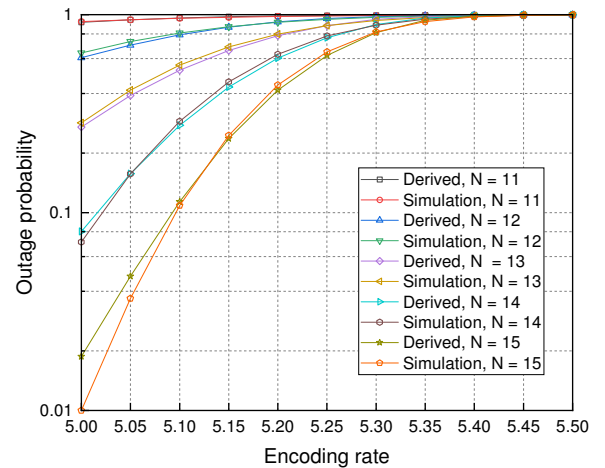


Fig. 10. Outage probability under FZF precoding with different number of antennas each AP. System parameters: $M = 120$, $l_p = 10$.

As anticipated, the outage probability increases continuously with higher coding rates and a reduced number of antennas on the APs. Moreover, it is noteworthy that our derived results closely align with the results obtained from Monte Carlo simulations across various scenarios.

VI. CONCLUSION

In this paper, we provided the PDF and CDF of the SINR in CF mMIMO systems considering both MRT and FZF precoding schemes. Moreover, we have performed a comprehensive performance analysis based on these results. Specifically, we modeled a CF mMIMO system with pilot contamination and derived the expression for the SINR. Then, by considering the independence of the signals, we divided the SINR into two components, i.e., DS and IN. Under MRT precoding, we derived the distributions of DS and IN using CLT and random matrix theory, enabling the analysis of the distribution of the SINR. Under FZF precoding, we directly computed the DS and derived the distribution of IN, which allowed us to obtain the PDF and CDF of the SINR. Based on the aforementioned analysis, we derived expressions for the achievable rate and the outage probability in CF mMIMO systems under MRT and FZF precoding, respectively. Finally, simulation results demonstrated the accuracy of our derivations.

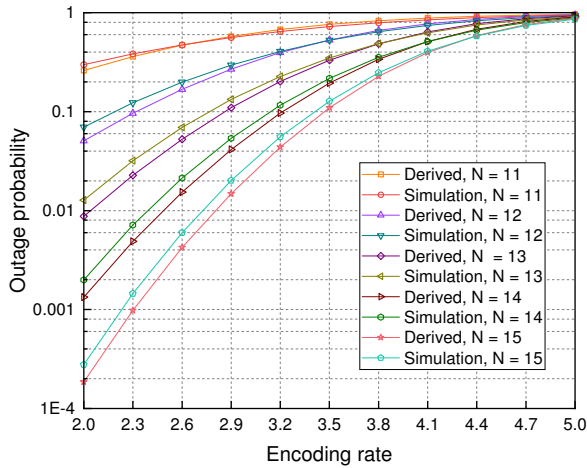


Fig. 11. Outage probability under MRT precoding with different number of antennas each AP. System parameters: $M = 120$, $l_p = 10$.

Currently, research on the statistical characteristics of SINR in the CF mMIMO system is still in its preliminary stage, and further investigation is required. Firstly, when deploying other precoding schemes, such as local ZF or MMSE precoding, in CF mMIMO systems, the corresponding SINR distributions also need to be analyzed. Secondly, in a more realistic CF mMIMO system, factors such as backhaul constraints and hardware impairments must be considered to evaluate their impact on the SINR distribution and derive appropriate models. Lastly, it would be a meaningful endeavor to design new power allocation schemes, pilot allocation schemes, and other system design schemes based on the SE and EE derived from our current analysis of the statistical characteristics of SINR in CF mMIMO systems. These endeavors aim to better harness the potential of CF mMIMO systems.

APPENDIX A PROOF OF LEMMA 1

When MRT precoding is used for downlink data transmission, the precoding vector can be expressed as

$$\mathbf{b}_{mk} = \frac{\bar{\mathbf{H}}_m \mathbf{e}_{ik}}{\sqrt{\mathbb{E} \left\{ \left\| \bar{\mathbf{H}}_m \mathbf{e}_{ik} \right\|^2 \right\}}} = \frac{\hat{\mathbf{h}}_{mk}}{\sqrt{N c_{mk}}}. \quad (38)$$

Estimated channel $\hat{\mathbf{h}}_{mk}$ follows the distribution of $\mathcal{CN}(0, c_{mk} \mathbf{I}_N)$, then $\xi_{mk} = \sqrt{\frac{\eta_{mk}}{N c_{mk}}} \hat{\mathbf{h}}_{mk}^H \hat{\mathbf{h}}_{mk}$ follows Gamma distribution with shape parameter N and scale parameter $\sqrt{\frac{\eta_{mk} c_{mk}}{N}}$, i.e., $\xi_{mk} \sim \text{Gamma}(N, \sqrt{\frac{\eta_{mk} c_{mk}}{N}})$.

Then the first moment to fourth moment of ξ_{mk} can be expressed as follows:

$$\mathbb{E} \{ \xi_{mk} \} = \sqrt{N \eta_{mk} c_{mk}}, \quad (39a)$$

$$\mathbb{E} \{ \xi_{mk}^2 \} = (N + 1) \eta_{mk} c_{mk}, \quad (39b)$$

$$\mathbb{E} \{ \xi_{mk}^3 \} = \frac{(N + 1)(N + 2)}{\sqrt{N}} \eta_{mk}^{\frac{3}{2}} c_{mk}^{\frac{3}{2}}, \quad (39c)$$

$$\mathbb{E} \{ \xi_{mk}^4 \} = \frac{(N + 1)(N + 2)(N + 3)}{N} \eta_{mk}^2 c_{mk}^2. \quad (39d)$$

The first moment of the $U_k^1 = \left| \sum_{m \in \mathcal{M}} \xi_{mk} \right|^2$ can be expressed as follows:

$$\begin{aligned} u_{U_k^1} &= \mathbb{E} \{ U_k^1 \} \\ &= \mathbb{E} \left\{ \left| \sum_{m \in \mathcal{M}} \xi_{mk} \right|^2 \right\} \stackrel{(a)}{=} \mathbb{E} \left\{ \left(\sum_{m \in \mathcal{M}} \xi_{mk} \right)^2 \right\} \\ &\stackrel{(b)}{=} \sum_{m \in \mathcal{M}} \mathbb{E} \{ \xi_{mk}^2 \} + \sum_{m \in \mathcal{M}} \sum_{m_1 \neq m} \mathbb{E} \{ \xi_{mk} \} \mathbb{E} \{ \xi_{m_1 k} \}, \end{aligned} \quad (40)$$

where (a) follows the fact that ξ_{mk} is real variable, and (b) is obtained based on the independence between ξ_{mk} and $\xi_{m_1 k}$ when $m \neq m_1$. By inserting (39a) and (39b) into (40), we can obtain the first moment of the U_k^1 .

Similarly, the second moment of U_k^1 is given in (41). The second moment of U_k^1 is obtained by using (39a)-(39d) and (41).

APPENDIX B PROOF OF LEMMA 2

According to (7), users using the same pilot sequence have the parallel estimated channels. Thus the first and second moments of $U_{kk_1}^2$ can be obtained similarly to U_k^1 when user k and user k_1 use the same pilot sequence. The first to fourth moment of ξ_{mkk_1} can be calculated as follows:

$$\mathbb{E} \{ \xi_{mkk_1} \} = \sqrt{N \eta_{mk_1} c_{mk}}, \quad (42a)$$

$$\mathbb{E} \{ \xi_{mkk_1}^2 \} = (N + 1) \eta_{mk_1} c_{mk}, \quad (42b)$$

$$\mathbb{E} \{ \xi_{mkk_1}^3 \} = \frac{(N + 1)(N + 2)}{\sqrt{N}} \eta_{mk_1}^{\frac{3}{2}} c_{mk}^{\frac{3}{2}}, \quad (42c)$$

$$\mathbb{E} \{ \xi_{mkk_1}^4 \} = \frac{(N + 1)(N + 2)(N + 3)}{N} \eta_{mk_1}^2 c_{mk}^2. \quad (42d)$$

Then the first moment of $U_{kk_1}^2$ can be expressed as follows:

$$\begin{aligned} \mathbb{E} \{ U_{kk_1}^2 \} &= \\ &= \sum_{m \in \mathcal{M}} \mathbb{E} \{ \xi_{mkk_1}^2 \} + \sum_{m \in \mathcal{M}} \sum_{m_1 \neq m} \mathbb{E} \{ \xi_{mkk_1} \} \mathbb{E} \{ \xi_{m_1 k k_1} \} \end{aligned} \quad (43)$$

The second moment of $U_{kk_1}^2$ is given in (44). The first and second moments of $U_{kk_1}^2$ can be obtained by using (42), (43) and (44).

When user k and user k_1 use different pilot sequences, i.e., $k_1 \notin \mathcal{P}_k$, the second and fourth moment of ξ_{mkk_1} can be expressed as follows:

$$\mathbb{E} \{ \xi_{mkk_1}^* \xi_{mkk_1} \} = \eta_{mk_1} c_{mk}, \quad (45a)$$

$$\mathbb{E} \left\{ \left(\xi_{mkk_1}^* \xi_{mkk_1} \right)^2 \right\} = \frac{2(N + 1)}{N} \eta_{mk_1}^2 c_{mk}^2, \quad (45b)$$

The first moment of $U_{kk_1}^2$ when $k_1 \notin \mathcal{P}_k$ can be expressed as follows:

$$\begin{aligned} \mathbb{E} \{ U_{kk_1}^2 \} &= \mathbb{E} \left\{ \left(\sum_{m \in \mathcal{M}} \xi_{mkk_1}^* \right) \left(\sum_{m \in \mathcal{M}} \xi_{mkk_1} \right) \right\} \\ &= \sum_{m \in \mathcal{M}} \mathbb{E} \{ \xi_{mkk_1}^* \xi_{mkk_1} \} + \sum_{m \in \mathcal{M}} \sum_{m_1 \neq m} \mathbb{E} \{ \xi_{mkk_1}^* \xi_{m_1 k k_1} \} \\ &\stackrel{(a)}{=} \sum_{m \in \mathcal{M}} \mathbb{E} \{ \xi_{mkk_1}^* \xi_{mkk_1} \} \end{aligned} \quad (46)$$

$$\begin{aligned}
u_{U_k^1}^{(2)} &= \mathbb{E} \left\{ (U_k^1)^2 \right\} = \mathbb{E} \left\{ \left| \sum_{m \in \mathcal{M}} \xi_{mk} \right|^4 \right\} = \mathbb{E} \left\{ \left(\sum_{m \in \mathcal{M}} \xi_{mk} \right)^4 \right\} = \mathbb{E} \left\{ \left(\sum_{m \in \mathcal{M}} \xi_{mk}^2 + \sum_{m \in \mathcal{M}} \sum_{m_1 \neq m} \xi_{mk} \xi_{m_1 k} \right)^2 \right\} \\
&= \sum_{m \in \mathcal{M}} \mathbb{E} \{ \xi_{mk}^4 \} + \sum_{m \in \mathcal{M}} \sum_{m_1 \neq m} \sum_{m_2 \neq m, m_1} 6 \mathbb{E} \{ \xi_{mk}^2 \} \mathbb{E} \{ \xi_{m_1 k} \} \mathbb{E} \{ \xi_{m_2 k} \} + \sum_{m \in \mathcal{M}} \sum_{m_1 \neq m} 4 \mathbb{E} \{ \xi_{mk}^3 \} \mathbb{E} \{ \xi_{m_1 k} \} \\
&+ \sum_{m \in \mathcal{M}} \sum_{m_1 \neq m} 3 \mathbb{E} \{ \xi_{mk}^2 \} \mathbb{E} \{ \xi_{m_1 k}^2 \} + \sum_{m \in \mathcal{M}} \sum_{m_1 \neq m} \sum_{m_2 \neq m, m_1} \sum_{m_3 \neq m, m_1, m_2} \mathbb{E} \{ \xi_{mk} \} \mathbb{E} \{ \xi_{m_1 k} \} \mathbb{E} \{ \xi_{m_2 k} \} \mathbb{E} \{ \xi_{m_3 k} \}.
\end{aligned} \tag{41}$$

$$\begin{aligned}
\mathbb{E} \left\{ (U_{kk_1}^2)^2 \right\} &= \sum_{m \in \mathcal{M}} \mathbb{E} \{ \xi_{mkk_1}^4 \} + \sum_{m \in \mathcal{M}} \sum_{m_1 \neq m} \sum_{m_2 \neq m, m_1} 6 \mathbb{E} \{ \xi_{mkk_1}^2 \} \mathbb{E} \{ \xi_{m_1 k k_1} \} \mathbb{E} \{ \xi_{m_2 k k_1} \} \\
&+ \sum_{m \in \mathcal{M}} \sum_{m_1 \neq m} 4 \mathbb{E} \{ \xi_{mkk_1}^3 \} \mathbb{E} \{ \xi_{m_1 k k_1} \} + \sum_{m \in \mathcal{M}} \sum_{m_1 \neq m} 3 \mathbb{E} \{ \xi_{mkk_1}^2 \} \mathbb{E} \{ \xi_{m_1 k k_1}^2 \} \\
&+ \sum_{m \in \mathcal{M}} \sum_{m_1 \neq m} \sum_{m_2 \neq m, m_1} \sum_{m_3 \neq m, m_1, m_2} \mathbb{E} \{ \xi_{mkk_1} \} \mathbb{E} \{ \xi_{m_1 k k_1} \} \mathbb{E} \{ \xi_{m_2 k k_1} \} \mathbb{E} \{ \xi_{m_3 k k_1} \}.
\end{aligned} \tag{44}$$

$$\begin{aligned}
\mathbb{E} \left\{ (U_{kk_1}^2)^2 \right\} &= \mathbb{E} \left\{ \left| \sum_{m \in \mathcal{M}} \xi_{mkk_1} \right|^4 \right\} = \mathbb{E} \left\{ \left(\sum_{m \in \mathcal{M}} \xi_{mkk_1}^* \xi_{mkk_1} + \sum_{m \in \mathcal{M}} \sum_{m_1 \neq m} \xi_{mkk_1}^* \xi_{m_1 k k_1} \right)^2 \right\} \\
&= \sum_{m \in \mathcal{M}} \mathbb{E} \left\{ (\xi_{mkk_1}^* \xi_{mkk_1})^2 \right\} + 2 \sum_{m \in \mathcal{M}} \sum_{m_1 \neq m} \mathbb{E} \{ \xi_{mkk_1}^* \xi_{mkk_1} \} \mathbb{E} \{ \xi_{m_1 k k_1}^* \xi_{m_1 k k_1} \}.
\end{aligned} \tag{47}$$

where (a) is obtained based on the fact that the exception of ξ_{mkk_1} is zero when user k and user k_1 use different pilot sequences and the independence between ξ_{mkk_1} and $\xi_{m_1 k k_1}$ when $m \neq m_1$. Then the second moment of $U_{kk_1}^2$ when user k and user k_1 use different pilot sequences is given in (47).

By using (45), (46) and (47), we can obtain the first and second moment of $U_{kk_1}^2$ when $k_1 \notin \mathcal{P}_k$.

We calculated the first and second moments of $U_{kk_1}^3$ using a similar way with $U_{kk_1}^2$. The second and fourth moment of ψ_{mkk_1} can be calculated as follows:

$$\begin{aligned}
\mathbb{E} \{ \psi_{mkk_1}^* \psi_{mkk_1} \} &= \eta_{m k_1} (\beta_{mk} - c_{mk}), \\
\mathbb{E} \left\{ (\psi_{mkk_1}^* \psi_{mkk_1})^2 \right\} &= \frac{2(N+1)}{N} \eta_{m k_1}^2 (\beta_{mk} - c_{mk})^2,
\end{aligned} \tag{48}$$

Then the first and second moment of $U_{kk_1}^3$ can be expressed as follow:

$$\begin{aligned}
\mathbb{E} \{ U_{kk_1}^3 \} &= \sum_{m \in \mathcal{M}} \mathbb{E} \{ \psi_{mkk_1}^* \psi_{mkk_1} \}, \\
\mathbb{E} \left\{ (U_{kk_1}^3)^2 \right\} &= \sum_{m \in \mathcal{M}} \mathbb{E} \left\{ (\psi_{mkk_1}^* \psi_{mkk_1})^2 \right\} \\
&+ 2 \sum_{m \in \mathcal{M}} \sum_{m_1 \neq m} \mathbb{E} \{ \psi_{mkk_1}^* \psi_{mkk_1} \} \mathbb{E} \{ \psi_{m_1 k k_1}^* \psi_{m_1 k k_1} \}.
\end{aligned} \tag{49}$$

The first and second moment of $U_{kk_1}^3$ can be obtained by using (48) and (49). The first order of IN_k^{FZF} can be expressed as

follows:

$$u_{\text{IN}_k^{\text{FZF}}} = \rho_d \sum_{k_1 \neq k} \mathbb{E} \{ U_{kk_1}^2 \} + \rho_d \sum_{k_1 \in \mathcal{K}} \mathbb{E} \{ U_{kk_1}^3 \} + 1. \tag{50}$$

The second moments of IN_k^{FZF} can be expressed as

Then the first and second moments of IN_k^{FZF} can be obtained.

APPENDIX C PROOF OF THEOREM 1

In the CF mMIMO system with MRT precoding, the distribution of DS_k^{MRT} can be approximated as a Gamma distribution with shape parameter j_{k_1} and scale parameter $\rho_d \chi_{k_1}$ for user k , and IN_k^{MRT} can be seemed as Gamma distribution with shape parameter j_{k_1} and scale parameter χ_{k_2} . Since the $\rho_d U_{k_1}$ and IN_k^{MRT} are independent with each other. The CDF of γ_k can be calculated as follows:

$$\begin{aligned}
P \{ \gamma_k \leq x \} &= P \left\{ \frac{\text{DS}_k^{\text{MRT}}}{\text{IN}_k^{\text{MRT}}} \leq x \right\} = P \{ \text{DS}_k^{\text{MRT}} \leq \text{IN}_k^{\text{MRT}} x \} \\
&= \int_0^\infty F_{\text{DS}_k^{\text{MRT}}}(x x_1) f_{\text{IN}_k^{\text{MRT}}}(x_1) dx_1.
\end{aligned} \tag{52}$$

where $F_{\text{DS}_k^{\text{MRT}}}(\cdot)$ denotes the CDF of DS_k^{MRT} and $f_{\text{IN}_k^{\text{MRT}}}(\cdot)$ represents the PDF of IN_k^{MRT} . Then the PDF of γ_k can be calculated based on (52), which is given in (53)

Based on the PDF of γ_k , the CDF of γ_k can be calculated using $F_{\gamma_k}^{\text{MRT}}(x) = \int_0^x f_{\gamma_k}^{\text{MRT}}(x_1) dx_1$ directly.

$$\begin{aligned}
u_{\text{INFZF}}^{(2)} &= \mathbb{E} \left\{ \left(\rho_d \sum_{k_1 \neq k} U_{kk_1}^2 + \rho_d \sum_{k_1 \in \mathcal{K}} U_{kk_1}^3 + z_k \right)^2 \right\} \\
&= \rho_d^2 \left(\sum_{k_1 \neq k} \mathbb{E} \{ (U_{kk_1}^2)^2 \} + \sum_{k_1 \neq k} \sum_{k_2 \neq k, k_1} \mathbb{E} \{ U_{kk_1}^2 \} \mathbb{E} \{ U_{kk_2}^2 \} + \sum_{k_1 \in \mathcal{K}} \mathbb{E} \{ (U_{kk_1}^3)^2 \} + 2 \right. \\
&\quad \left. + \sum_{k_1 \in \mathcal{K}} \sum_{k_2 \neq k_1} \mathbb{E} \{ U_{kk_1}^3 \} \mathbb{E} \{ U_{kk_2}^3 \} + 2 \left(\sum_{k_1 \neq k} \mathbb{E} \{ U_{kk_1}^2 \} \right) \left(\sum_{k_1 \in \mathcal{K}} \mathbb{E} \{ U_{kk_1}^3 \} \right) \right) + 2\rho_d \left(\sum_{k_1 \neq k} \mathbb{E} \{ U_{kk_1}^2 \} + \sum_{k_1 \in \mathcal{K}} \mathbb{E} \{ U_{kk_1}^3 \} \right). \tag{51}
\end{aligned}$$

$$\begin{aligned}
f_{\gamma_k}^{\text{MRT}}(x) &= \frac{dP\{\gamma_k \leq x\}}{dx} = \int_0^\infty x_1 f_{\text{DS}_k^{\text{MRT}}}(xx_1) f_{\text{IN}_k^{\text{MRT}}}(x_1) dx_1. \\
&= \int_0^\infty x_1 \frac{1}{\Gamma(j_{k1}) (\rho_d \chi_{k1})^{j_{k1}}} (xx_1)^{(j_{k1}-1)} e^{-\frac{xx_1}{\chi_{k1}}} \frac{1}{\Gamma(j_{k2}) (\chi_{k2})^{j_{k2}}} (x_1)^{(j_{k2}-1)} e^{-\frac{x_1}{\chi_{k2}}} dx_1 \\
&= \frac{\Gamma(j_{k1} + j_{k2})}{\Gamma(j_{k1}) \Gamma(j_{k2}) (\rho_d \chi_{k1})^{j_{k1}} \chi_{k2}^{j_{k2}}} x^{j_{k1}-1} \left(\frac{1}{\chi_{k2}} + \frac{x}{\rho_d \chi_{k1}} \right)^{-j_{k1}-j_{k2}}. \tag{53}
\end{aligned}$$

REFERENCES

- [1] K. Zheng, L. Zhao, J. Mei, B. Shao, W. Xiang, and L. Hanzo, "Survey of large-scale MIMO systems," *IEEE Commun. Surveys Tuts.*, vol. 17, no. 3, pp. 1738–1760, 3rd Quart., 2015.
- [2] H. Pei, X. Chen, X. Huang, X. Liu, X. Zhang, and Y. Huang, "Key issues and algorithms of multiple-input-multiple-output over-the-air testing in the multi-probe anechoic chamber setup," *Sci. China Inf. Sci.*, vol. 65, no. 3, p. 131302, 2022.
- [3] R. Feng, C.-X. Wang, J. Huang, and X. Gao, "Recent advances of ultramassive multiple-input, multiple-output technologies: Realizing a sixth-generation future in spatial and beam domains," *IEEE Veh. Technol. Mag.*, vol. 18, no. 1, pp. 70–79, Mar. 2023.
- [4] S. Elhoushy, M. Ibrahim, and W. Hamouda, "Cell-free massive MIMO: A survey," *IEEE Commun. Surveys Tuts.*, vol. 24, no. 1, pp. 492–523, 1st Quart., 2022.
- [5] A. Lozano, R. W. Heath, and J. G. Andrews, "Fundamental limits of cooperation," *IEEE Trans. Inf. Theory*, vol. 59, no. 9, pp. 5213–5226, Sep. 2013.
- [6] F. Guo, H. Lu, and Z. Gu, "Joint power and user grouping optimization in cell-free massive MIMO systems," *IEEE Trans. Wireless Commun.*, vol. 21, no. 2, pp. 991–1006, Feb. 2022.
- [7] J. Zhang, S. Chen, Y. Lin, J. Zheng, B. Ai, and L. Hanzo, "Cell-free massive MIMO: A new next-generation paradigm," *IEEE Access*, vol. 7, pp. 99 878–99 888, Jul. 2019.
- [8] Z. Chen and E. Björnson, "Channel hardening and favorable propagation in cell-free massive MIMO with stochastic geometry," *IEEE Trans. Commun.*, vol. 66, no. 11, pp. 5205–5219, Nov. 2018.
- [9] E. Nayebi, A. Ashikhmin, T. L. Marzetta, H. Yang, and B. D. Rao, "Precoding and power optimization in cell-free massive MIMO systems," *IEEE Trans. Wireless Commun.*, vol. 16, no. 7, pp. 4445–4459, Jul. 2017.
- [10] H. Q. Ngo, L.-N. Tran, T. Q. Duong, M. Matthaiou, and E. G. Larsson, "On the total energy efficiency of cell-free massive MIMO," *IEEE Trans. Green Commun. Netw.*, vol. 2, no. 1, pp. 25–39, Mar. 2018.
- [11] H. Q. Ngo, A. Ashikhmin, H. Yang, E. G. Larsson, and T. L. Marzetta, "Cell-free massive MIMO versus small cells," *IEEE Trans. Wireless Commun.*, vol. 16, no. 3, pp. 1834–1850, Mar. 2017.
- [12] G. Interdonato, M. Karlsson, E. Björnson, and E. G. Larsson, "Local partial zero-forcing precoding for cell-free massive MIMO," *IEEE Trans. Wireless Commun.*, vol. 19, no. 7, pp. 4758–4774, Jul. 2020.
- [13] J. Zhang, J. Zhang, E. Björnson, and B. Ai, "Local partial zero-forcing combining for cell-free massive MIMO systems," *IEEE Trans. Commun.*, vol. 69, no. 12, pp. 8459–8473, Dec. 2021.
- [14] E. Nayebi, A. Ashikhmin, T. L. Marzetta, and B. D. Rao, "Performance of cell-free massive MIMO systems with MMSE and LSFD receivers," in *Proc. 50th Asilomar Conf. Signals, Syst. Comput.*, Nov. 2016, pp. 203–207.
- [15] Z. Wang, J. Zhang, B. Ai, C. Yuen, and M. Debbah, "Uplink performance of cell-free massive MIMO with multi-antenna users over jointly-correlated rayleigh fading channels," *IEEE Trans. Wireless Commun.*, vol. 21, no. 9, pp. 7391–7406, Sep. 2022.
- [16] J. Zheng, J. Zhang, J. Cheng, V. C. M. Leung, D. W. K. Ng, and B. Ai, "Asynchronous cell-free massive MIMO with rate-splitting," *IEEE J. Sel. Areas Commun.*, vol. 41, no. 5, pp. 1366–1382, May. 2023.
- [17] A. Papazafeiropoulos, P. Kourtessis, M. D. Renzo, S. Chatzinotas, and J. M. Senior, "Performance analysis of cell-free massive MIMO systems: A stochastic geometry approach," *IEEE Trans. Veh. Commun.*, vol. 69, no. 4, pp. 3523–3537, Apr. 2020.
- [18] O. Özdogan, E. Björnson, and J. Zhang, "Performance of cell-free massive MIMO with rician fading and phase shifts," *IEEE Trans. Wireless Commun.*, vol. 18, no. 11, pp. 5299–5315, Nov. 2019.
- [19] Y. Fang, L. Qiu, X. Liang, and C. Ren, "Cell-free massive MIMO systems with oscillator phase noise: Performance analysis and power control," *IEEE Trans. Veh. Commun.*, vol. 70, no. 10, pp. 10048–10064, Oct. 2021.
- [20] H. Masoumi and M. J. Emadi, "Performance analysis of cell-free massive MIMO system with limited fronthaul capacity and hardware impairments," *IEEE Trans. Wireless Commun.*, vol. 19, no. 2, pp. 1038–1053, Feb. 2020.
- [21] Y. Zhang, M. Zhou, X. Qiao, H. Cao, and L. Yang, "On the performance of cell-free massive MIMO with low-resolution ADCs," *IEEE Access*, vol. 7, pp. 117 968–117 977, Aug. 2019.
- [22] B. Al-Nahhas, M. Obeed, A. Chaaban, and M. J. Hossain, "Ris-aided cell-free massive MIMO: Performance analysis and competitiveness," in *Proc. IEEE Int. Conf. Commun. Workshops (ICC Workshops)*, Jun. 2021, pp. 1–6.
- [23] S. Kusaladharna, W.-P. Zhu, W. Ajib, and G. A. A. Baduge, "Stochastic geometry based performance characterization of swipt in cell-free massive MIMO," *IEEE Trans. Veh. Commun.*, vol. 69, no. 11, pp. 13 357–13 370, Nov. 2020.
- [24] Y. Li and G. A. Aruma Baduge, "NOMA-aided cell-free massive MIMO systems," *IEEE Wireless Commun. Lett.*, vol. 7, no. 6, pp. 950–953, Dec. 2018.
- [25] A. Mishra, Y. Mao, L. Sanguinetti, and B. Clerckx, "Rate-splitting assisted massive machine-type communications in cell-free massive MIMO," *IEEE Commun. Lett.*, vol. 26, no. 6, pp. 1358–1362, Jun. 2022.
- [26] P. Li, D. Paul, R. Narasimhan, and J. Cioffi, "On the distribution of

- SINR for the MMSE MIMO receiver and performance analysis," *IEEE Trans. Inf. Theory*, vol. 52, no. 1, pp. 271–286, Jan. 2006.
- [27] H. Lim and D. Yoon, "On the Distribution of SINR for MMSE MIMO Systems," *IEEE Trans. Commun.*, vol. 67, no. 6, pp. 4035–4046, Jun. 2019.
- [28] H. Q. Ngo, E. G. Larsson, and T. L. Marzetta, "Energy and spectral efficiency of very large multiuser MIMO systems," *IEEE Trans. Commun.*, vol. 61, no. 4, pp. 1436–1449, Apr. 2013.
- [29] Y. Jiang, M. K. Varanasi, and J. Li, "Performance analysis of ZF and MMSE equalizers for MIMO systems: An in-depth study of the high snr regime," *IEEE Trans. Inf. Theory*, vol. 57, no. 4, pp. 2008–2026, Apr. 2011.
- [30] Z. Zhang, X. You, D. Wang, X. Xia, P. Zhu, Y. Jiang, C. Liang, and J. Wang, "Performance of multidevice downlink cell-free system under finite blocklength for uRLLC with hard deadlines," *IEEE J. Sel. Areas Commun.*, pp. 1–1, 2023.
- [31] X. Zhang, J. Wang, and H. V. Poor, "Statistical delay and error-rate bounded qos provisioning for mURLLC over 6g cf M-MIMO mobile networks in the finite blocklength regime," *IEEE J. Sel. Areas Commun.*, vol. 39, no. 3, pp. 652–667, Mar. 2021.
- [32] Wolfram. Hypergeometric function. [Online]. Available: <https://reference.wolfram.com/language/ref/Hypergeometric2F1.html>
- [33] A. Edelman and N. R. Rao, "Random matrix theory," *Acta Numer.*, vol. 14, p. 233–297, 2005.
- [34] Wolfram. Generalized hypergeometric function. [Online]. Available: <https://reference.wolfram.com/language/ref/HypergeometricPFQ.html>